CHIN. PHYS. LETT. Vol. 36, No. 2 (2019) 028401

# Ultrafast Carrier Dynamics and Terahertz Photoconductivity of Mixed-Cation and Lead Mixed-Halide Hybrid Perovskites *

Wan-Ying Zhao(赵婉莹)[1], Zhi-Liang Ku(库治良)[2], Li-Ping Lv(吕丽萍)[3], Xian Lin(林贤)[1], Yong Peng(彭勇)[2], Zuan-Ming Jin(金钻明)[1,4**], Guo-Hong Ma(马国宏)[1,4**], Jian-Quan Yao(姚建铨)[5]

[1]*Department of Physics, Shanghai University, Shanghai 200444*
[2]*State Key Laboratory of Advanced Technology for Materials Synthesis and Processing, Wuhan University of Technology, Wuhan 430070*
[3]*Department of Chemical Engineering, School of Environmental and Chemical Engineering, Shanghai University, Shanghai 200444*
[4]*STU & SIOM Joint Laboratory for Superintense Lasers and Applications, Shanghai 201210*
[5]*College of Precision Instrument and Opto-electronics Engineering, Institute of Laser and Opto-electronics, Tianjin University, Tianjin 300072*

(Received 5 September 2018)

*Using time-dependent terahertz spectroscopy, we investigate the role of mixed-cation and mixed-halide on the ultrafast photoconductivity dynamics of two different methylammonium (MA) lead-iodide perovskite thin films. It is found that the dynamics of conductivity after photoexcitation reveals significant correlation on the microscopy crystalline features of the samples. Our results show that mixed-cation and lead mixed-halide affect the charge carrier dynamics of the lead-iodide perovskites. In the (5-AVA)$_{0.05}$(MA)$_{0.95}$PbI$_{2.95}$Cl$_{0.05}$/spiro thin film, we observe a much weaker saturation trend of the initial photoconductivity with high excitation fluence, which is attributed to the combined effect of sequential charge carrier generation, transfer, cooling and polaron formation.*

*PACS: 84.60.Jt, 78.47.−p, 07.57.Ty* DOI: 10.1088/0256-307X/36/2/028401

In the past few years, hybrid organic-inorganic lead trihalide perovskite ($APbX_3$), such as methylammonium lead triiodide ($MAPbI_3$), has received an enormous amount of attention for thin film solar cell materials with efficient light absorption.[1,2] Due to strong light absorption and long charge diffusion length, $MAPbI_3$ shows superior photovoltaic properties with marked defect tolerance.[3–5] The power conversion efficiency (PCE) of the solar cell based on hybrid organic-inorganic perovskite film has increased from 10% to 23% in the past few years.[2,6–11] In addition, it is reported that the external quantum efficiency of perovskite reaches 20.3%.[12] This represents a substantial step towards the practical application of perovskite LEDs in lighting and display.[12,13] The stability for the reproducible high efficiency is a major concern towards industrialization. Meanwhile, a large body of work has been devoted to understanding 'why' lead halide perovskites own long carrier lifetimes, large carrier diffusion length and high defect-tolerance. Recently, several groups suggest that a reduced coulomb attraction of the carriers due to the formation of large polarons in the hybrid organic-inorganic lead-iodide perovskites can be regarded as a possible mechanism for the large diffusion length of photo-carriers.[14–16]

The crystalline of hybrid organic-inorganic lead halide perovskite structure can be viewed as two interpenetrating sublattices, including the organic sublattice $CH_3NH_3^+$ and the inorganic Pb halide octahedral $PbX_3^-$ sublattice. Generally, both the valence and conduction bands related to charge transport are formed by the inorganic $PbX_3^-$ sublattice. However, the organic $CH_3NH_3^+$ sublattice serves as a medium to modulate the electrostatic landscape experienced by the charge carriers, which could lead to charge screening and localization. To understand photo-induced carrier conductivity and its dynamics, it is very important to identify the role of mixed organic cations and mixed halides anions in this organic-inorganic hybrid peroviskite. To date, the best perovskite solar cells were fabricated using mixed organic cations and mixed halides, which behave higher light harvesting capability, longer charge diffusion length and superior photo-stability than the prototypical pervoskite film, $MAPbI_3$.[17,18]

Recently, Mei *et al.* fabricated a perovskite solar cell with a mixed-cation perovskite (5-AVA)$_x$(MA)$_{1-x}$PbI$_3$, where (5-AVA) is the abbreviation of 5-ammoniumvaleric acid. As compared to $MAPbI_3$, the (5-AVA)$_x$(MA)$_{1-x}$PbI$_3$ was characterized to have a longer exciton lifetime and a higher quantum yield for photoinduced charge separation.[19] Pei *et al.* reported that the PCE and photo-durability in (5-AVA)$_y$(MA)$_{1-y}$PbI$_{3-x}$Cl$_x$ were higher than that of (5-AVA)$_x$(MA)$_{1-x}$PbI$_3$.[18] A possible mechanism behind the durability enhancement in (5-AVA)$_y$(MA)$_{1-y}$PbI$_{3-x}$Cl$_x$ perovskite was attributed to the crystallographic stability and carrier transport length.[20,21] Even though mixed-cation lead mixed-halide perovskites have lower defect concentration and higher stability, the understanding of doping effect on photo-excited carrier dynamics in (5-AVA)$_y$(MA)$_{1-y}$PbI$_{3-x}$Cl$_x$ is still lacking because most works have focused on material development and

*Supported by the National Natural Science Foundation of China under Grant Nos 11604202, 11674213, 61735010 and 51603119, the Young Eastern Scholar under Grant Nos QD2015020 and QD2016027, the Shanghai Rising-Star Program under Grant No 18QA1401700, the 'Chen Guang' Project under Grant Nos 16CG45 and 16CG46, the Shanghai Municipal Education Commission, and the Shanghai Education Development Foundation.
**Corresponding author. Email: physics_jzm@shu.edu.cn; ghma@staff.shu.edu.cn
© 2019 Chinese Physical Society and IOP Publishing Ltd

device optimization.

Ultrafast photoinduced time-dependent terahertz (THz) conductivity spectra offer a contact-free amperemeter with sub-picosecond time resolution, which have been used to access the carrier transport, such as carrier density, carrier momentum scattering time and the dynamics of photoconductivity.[22,23] In this study, we employ time-domain THz spectroscopy to characterize the THz photo-conductivity changes and its dynamics in prototypical, $(5\text{-AVA})^+$- and $Cl^-$-codoped $MAPbI_3$. The initial dynamics of the photoinduced conductivity reveals significant dependence on the mixed-cation and lead mixed-halide. We find an increased THz photoconductivity in $Cl^-$ and $(5\text{-AVA})^+$ codoped perovskite. In addition, we investigate the influence of mixed-cation and lead mixed-halide in the $(5\text{-AVA})_y(MA)_{1-y}PbI_{3-x}Cl_x$ on the initial values of the photoconductivity, which is largely attributed to a combined effect of generation, transfer and cooling of hot carriers, and polaron formation.

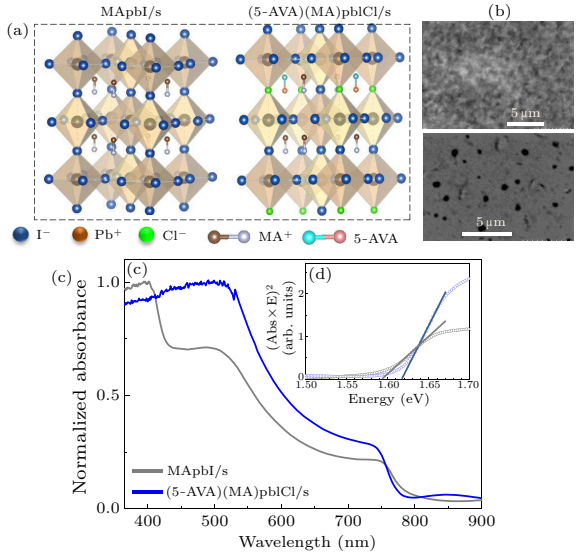


**Fig. 1.** (a) A schematic of the crystal structure of the two perovskite films: MAPbI/s and (5-AVA)(MA)PbICl/s. (b) Top-view SEM image of two perovskite films. The scale bar is 5 μm. (c) The normalized UV-visible absorption spectra, and (d) the Tauc plots of the two perovskite films, MAPbI/s and (5-AVA)(MA)PbICl/s.

As shown in Fig. 1(a), $MAPbI_3$/spiro-OMeTAD (MAPbI/s), and $(5\text{-AVA})_{0.05}(MA)_{0.95}PbI_{2.95}Cl_{0.05}$ /spiro-OMeTAD ((5-AVA)(MA)PbICl/s) perovskite films were deposited on fused silica substrates by 'one-step' spin-coating method.[19] For the $MAPbI_3$ sample, $MAPbI_3$ precursor solution was firstly prepared by mixing MAI (0.395 g) and $PbI_2$ (1.157 g) in DMF (2 mL) at 70℃ with stirring for 24 h. Then, the as-prepared precursor solution was spin-coated on the quartz slide at 3000 rpm, followed by drying at 100℃ in glove box. The color of the $MAPbI_3$ film turned from yellow to dark gradually, suggesting the removing of solvent and the formation of the $MAPbI_3$ perovskite multicrystalline film. On this basis, a $(5\text{-AVA}_{0.05}\,MA_{0.95})PbI_{2.95}Cl_{0.05}$ sample was prepared by replacing another 5% of the MAI by (5-AVA)I, which was synthesized according to the method reported by in the previous work.[19] In two sample systems, $(5\text{-AVA})_y(MA)_{1-y}PbI_{3-x}Cl_x$ is used as the light absorber, while spiro-OMeTAD is used as the hole transport layer. Our deposited films have average thicknesses of 400 nm±100 nm determined with a surface profilometer.

Figure 1(b) shows the surface scanning electron microscopy (SEM) images of the two samples. It is seen that the surface of MAPbI/s exhibits an irregular morphology with roughness. Indeed, manipulating the composition of $PbI_3^-$ by adding $Cl^-$ considerably smooth the surface and leads to the stabilization of the perovskite phase with a uniform and dense morphology.

Typical ultraviolet-visible optical absorption spectra at room temperature are shown in Fig. 1(c). All the films show roughly the same absorption edge of ∼760 nm. As shown in Fig. 1(d), the Tauc plots reveal that the optical bandgap is around 1.61 eV for all the films, which agrees with both the experimentally measured values ranging from 1.57 to 1.63 eV,[24–26] and results from density functional theory (DFT) calculations.[27] The very close bandgap values may be attributed to the low replacement of $(MA)^+$ by $(5\text{-AVA})^+$, and $I^-$ by $Cl^-$, as shown in Fig. 1(d). The XRD results in Fig. S1 demonstrate that our perovskite films have the tetragonal structure at room temperature, which are in agreement with the previous publication.[28]

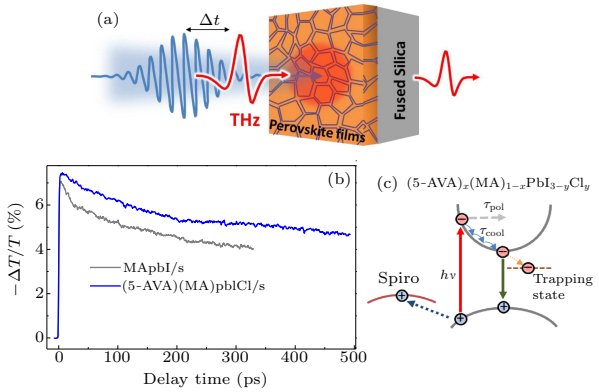


**Fig. 2.** (a) Schematic of optical-pump THz-probe spectroscopy for transient photo-conductivity measurements. (b) Time-resolved THz photoconductivity measurements of MAPbI/s and (5-AVA)(MA)PbICl/s at room temperature after photo-excitation at 400 nm. (c) Schematic diagram of the energy levels and charge carrier dynamics after photo-excitation in the perovskite/spiro-OMeTAD sample.

Our optical-pump THz-probe spectroscopy (OPTP) spectroscopy was driven by a Ti:sapphire femtosecond amplifier. The amplified fundamental beam centered at 800 nm (120 fs, 1 kHz) is split into two parts. One part of the laser output is used to generate and detect THz radiation by optical rectification and electro-optical sampling with two 1-mm-thick (110)-orientated ZnTe crystals. The other part is frequency doubled with a $\beta$-$BaB_2O_4$ crystal to deliver photo-energy of 3.1 eV (400 nm), which acts as a pump beam, as shown in Fig. 2(a). The photon energy of pump beam (3.1 eV) exceeds the dual valence band structure of all investigated samples. No significant degradation was observed during the experiments.

To avoid absorption of THz radiation due to water vapor, the setup was purged with dry nitrogen. A lock-in amplifier and an optical chopper were used to improve the signal-to-noise ratio in our measurements (see the supplementary material for details). All the experiments were performed at room temperature.

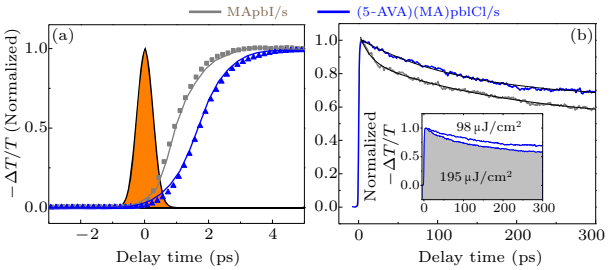


**Fig. 3.** (a) Comparison of the rise dynamics of the photoconductivity (normalized to unity) for two samples. The solid lines show the fits obtained from Eq. (1). The Gaussian instrument response function with FWHM of 120 fs is shown in orange. (b) The normalized $-\frac{\Delta T}{T}(\Delta t)$ for samples. The inset shows the normalized $-\frac{\Delta T}{T}(\Delta t)$ of (5-AVA)(MA)PbICl/s upon excitation at 400 nm with pump fluences of 98 and 195 μJ/cm$^2$. The black solid lines are multi-exponential fittings.

We plot the photo-induced peak change of the THz electric-field amplitude as a function of pump-probe time delay $-\frac{\Delta T}{T}(\Delta t)$, for MAPbI/s and (5-AVA)(MA)PbICl/s with a selected pump fluence of 98 μJ/cm$^2$, respectively. We show that $-\frac{\Delta T}{T}(\Delta t)$ keeps positive in all the samples, indicating the photo-induced absorption (positive photoconductivity) in all the perovskite films. After photo-excitation at 400 nm, $-\frac{\Delta T}{T}(\Delta t)$ exhibits an instantaneous rise and subsequently relaxation with hundreds of ps time scales. Actually, $-\frac{\Delta T}{T}(\Delta t)$ is correlated to the dynamics of real part of the photo-induced conductivity $\Delta\sigma$,[29,30] which will be discussed in the following. We therefore have shown that the photoconductivity increases during the first ∼1.5 ps after photoexcitation and then relaxes to a quasi-steady state. It is noted that the THz conductivity dynamics are dramatically different for samples, under the similar optical excitation condition (the excited sheet densities of $N_{\rm ex} = 3.2 \times 10^{17}$ photon/m$^2$). Not only the peak value but also the rise and relaxation dynamical response of $-\frac{\Delta T}{T}(\Delta t)$ are observably dependent on the mixed-cation and lead mixed-halide doping, as shown in Fig. 2(b). We find in our data that a small addition of chloride ions ($Cl^-$) to the (5-AVA)(MA)PbI results in a significant increase of photo-conductivity performance. The peak value of $-\frac{\Delta T}{T}(\Delta t)$ for (5-AVA)(MA)PbICl/s is larger than that for MAPbI/s. Our findings are indeed in agreement with the observed morphology of two perovskite films. As shown in Fig. 1(b), the (5-AVA)(MA)PbICl/s shows uniform and dense morphology, and the crystalline features have a much longer length scale than that of MAPbI/s. The well-developed crystallites of (5-AVA)(MA)PbICl/s lead to a reduced backscattering, less additional potential corrugations, and increasing average mobilities. This could be a possible reason for the increasing photoconductivity observed in (5-AVA)(MA)PbICl/s.

In addition, as mentioned in previous works, when the spiro-OMeTAD is introduced onto the top surface of the perovskite film, the hole injection from $(5\text{-AVA})_y(\text{MA})_{1-y}\text{PbI}_{3-x}\text{Cl}_x$ into spiro-OMeTAD occurs as a primary charge separation process at the interface,[31–33] as the blue dashed arrow shown in Fig. 2(c). The THz conductivity of the perovskite sample with spiro-OMeTAD is about 3–5 times smaller than that of the neat $\text{MAPbI}_3$.[31,33] The hole-injection process completes on the sub-picosecond time scale in MAPbI/s. Therefore, the photoconductivity measured in our sample systems comes mainly from the electrons left in the perovskite (light absorber layer). Certainly, it should be noted that the rise of $-\frac{\Delta T}{T}(\Delta t)$ could also be inevitably affected by the hole transfer at the interface between $(5\text{-AVA})_y(\text{MA})_{1-y}\text{PbI}_{3-x}\text{Cl}_x$ and spiro-OMeTAD.

THz transmission signal is not sensitive to the neutral exciton and is only affected by the charge carriers. Actually, the rise of photoconductivity is not limited by the generation of free carriers, which has been reported to occur on sub-100 fs timescales. For a bandgap excitation with a photoenergy of 3.1 eV, as shown in Fig. 2(c), the rapid rising of the photoconductivity shows a combined result: (1) the generation of mobile free electrons in the conduction band, (2) the charge carrier cooling (heat transfer to the lattice), which is determined by optical phonon emission, and (3) the formation of polarons (the dressing of carriers with phonons). As shown in Fig. 3(a), to quantify the observed rising of the THz photoconductivity, we employ a phenomenological model in which a rise component with two effective time constants and a mono-exponential decay with a time constant $\tau_{\rm decay}$ are given by[34,35]

$$\begin{aligned} -\frac{\Delta T}{T}(\Delta t) = {} & A \times \text{Conv}(e^{-t/\tau_{\rm decay}}, \tau_{\rm pulse}) \\ & + B \times \text{Conv}(e^{-t/\tau_{\rm decay}}, \tau_{\rm cooling}) \\ & + C \times \text{Conv}(e^{-t/\tau_{\rm decay}}, \tau_{\rm polaron}), \quad (1) \end{aligned}$$

where $\text{Conv}(e^{-t/\tau_{\rm decay}}, \tau)$ is the convolution of $e^{-t/\tau_{\rm decay}}$ with a Gaussian pulse ($\tau_{\rm pulse}$), carrier cooling time ($\tau_{\rm cooling}$), and polaron formation time ($\tau_{\rm polaron}$), respectively. The effective rise time is the amplitude-weight average of these three. Recently, Bretschneider *et al.* reported that the polaron behavior in lead-iodide perovskites originates from the coupling of charge carriers to lead-halide lattice rather than to organic cations.[36] Thus the timescale of polaron formation can be estimated simply from LO phonon oscillation period of 330 fs, which is consistent with their experimental result of about 400 fs.[36] From the fitting within the assumption of $\tau_{\rm polaron} = 400$ fs for MAPbI/s, the extracted cooling time $\tau_{\rm cooling} = 1.1 \pm 0.1$ ps are almost the same for two samples. Then, we fix $\tau_{\rm cooling} = 1.1$ ps and make $\tau_{\rm polaron}$ as a free fitting parameter for (5-AVA)(MA)PbICl/s. From the fitting, we obtain $\tau_{\rm polaron} = 0.45 \pm 0.02$ ps, which is around 10% larger than that of MAPbI.

As shown in Fig. 3(b), $-\frac{\Delta T}{T}(\Delta t)$ is normalized to unity, which allows us to compare the evolution

of the photoconductivity decay dynamics with multi-exponential fits. The previous studies showed that the carrier mobility remains constant for at least ∼1 ns.[37,38] As a matter of fact, the photo-carrier dynamics mainly includes three processes: monomolecular charge-recombination, bimolecular electron-hole recombination and the Auger recombination.[38,39] As shown in the inset of Fig. 3(b), the photo-carrier relaxation dynamics of (5-AVA)(MA)PbICl/s become faster under higher pump fluence, which indicates that a second-order recombination process involved.[39] In addition, it is found that the photo-carrier relaxation of MAPbI/s has an initial fast component compared to that of (5-AVA)(MA)PbICl/s under the similar excitation condition. In detail, the multi-exponential fits of the THz photoconductivity signals give a fast delay component of $\tau_1 \sim 50 \pm 3$ ps and a slow delay of $\tau_2 \sim 230 \pm 3$ ps for the MAPbI/s. In contrast, the photoconductivity decay for (5-AVA)(MA)PbICl/s can be well reproduced with a single exponential function with fitting lifetime of $1223 \pm 3$ ps. The fast component ($\tau_1 \sim 50 \pm 3$ ps) in MAPbI/s is typically related to the charge trapping by surface states,[40,41] as the orange arrow shown in Fig. 2(c). The disappearance of fast component in the doped perovskite films could be due to the unintentionally passivation by changing the mixed-cation of (5-AVA)(MA), and as a result, a better compactness, close-packed structure (as shown in Fig. 1(b)) is formed, which results in a reduction of surface recombination.

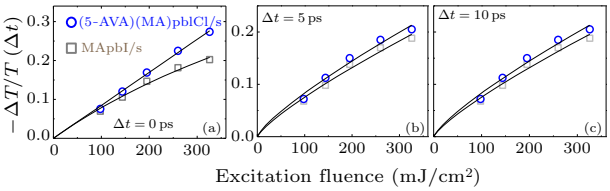


**Fig. 4.** The excitation-fluence-dependent $-\frac{\Delta T}{T}(\Delta t)$ of THz photoconductivity corresponding to time delay of (a) $\Delta t = 0$ ps (peak values), (b) $\Delta t = 5$ ps, and (c) $\Delta t = 10$ ps. The lines are guide for the eyes.

Figure 4 shows the peak amplitude of $-\frac{\Delta T}{T}(\Delta t)$ as a function of pump fluence (incident photo flux) ranging from 98 to 326 μJ/cm$^2$, which shows significantly different trends in prototypical MAPbI/s and codoping (5-AVA)(MA)PbICl/s films. We observe a sub-linear pump fluence dependence of $-\frac{\Delta T}{T}(\Delta t = 0\,\text{ps})$ in MAPbI/s, which is consistent with our previous work.[33] However, the initial photoconductivity follows a nearly linear relationship with pump fluence in (5-AVA)(MA)PbICl/s. It can be found that the different trends of $-\frac{\Delta T}{T}(\Delta t = 0\,\text{ps})$ between the MAPbI/s and the (5-AVA)(MA)PbICl/s become increasing larger under higher excitation densities, while the photoconductivities measured at $\Delta t = 5$ ps and $\Delta t = 10$ ps have similar excitation fluence dependences, as shown in Figs. 4(b) and 4(c). Therefore, the fluence-dependent initial photoconductivity can be explained by a combined effect of free carriers dissociated by excitons, free carriers transfer and cooling, and also the formation dynamics of a polaron. In detail, on the one hand, a stronger Coulomb screening means the larger dielectric constant and the lower exciton binding energy, which will consequently make it more easier for excitons dissociate into free carriers.[42,43] On the other hand, the polaron formation will result in an increasing effective mass by 20–45%, which could reduce the conductivity consequently.[44] Furthermore, the charge transport is also affected by the electron-phonon coupling constants.[45] Therefore, a laser pulse with shorter pulse width is required to distinguish each contribution of this combined effect, which is presently beyond the capabilities of our experiments.

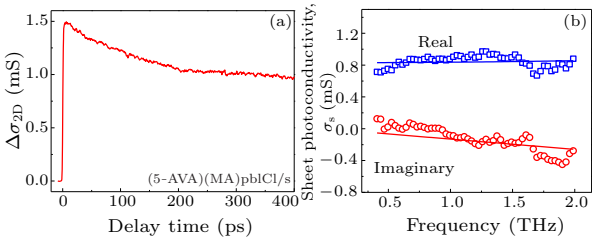


**Fig. 5.** (a) The transient sheet THz photoconductivity $\Delta\sigma_{2D}$ of (5-AVA)(MA)PbICl/s. (b) The real and imaginary parts of the photoconductivity spectrum for (5-AVA)(MA)PbICl/s, which are taken at $\Delta t = 5$ ps.

Finally, we acquire the dynamics of the real-part sheet photoconductivity $\Delta\sigma_{2D}$. As shown in Fig. 5(a), $\Delta\sigma_{2D}$ is reconstructed from $-\frac{\Delta T}{T}(\Delta t)$ using a thin-film approximation known as the Tinkham equation[46,47]

$$\Delta\sigma_{2D}(\Delta t) = (1+n)/Z_0[1/(1+\Delta T/T) - 1], \quad (2)$$

where $n$ is the refractive index of the material next to the photoexcited layer. In our case, the photoexcited layer is thinner than the sample, thus $n \approx 6$ is the THz refractive index of the perovskite film, as reported by Sendner *et al.*[45] $Z_0 = 377\,\Omega$ is the impedance of free space. The magnitude of $\Delta\sigma_{2D}$ is scaled to the product of the time-dependent carrier density and mobility of the photo-excited charge carriers. Figure 5(b) shows the flat real component of the measured photoconductivity with small negative imaginary component for (5-AVA)(MA)PbICl/s. Although the conductivity spectrum can be described by the Drude–Smith model, the photoconductivity reveals no significant frequency dependence within the 0.5–2 THz frequency window. This indicates that the carrier scattering time of all the samples is less than 20 fs.

In summary, we have demonstrated a comparative study of THz photo-conductivities of hybrid organic-inorganic lead halide perovskites. We have also investigated the role of the different doping extrinsic ions on the initial and relaxation dynamics of photoconductivity. The observed picosecond rise in the photoconductivity can be described by a combined effect of the generation, transfer, cooling of hot carriers, and also the formation of a polaron. Combined with the morphology analysis, we find that manipulating the composition of $PbI_3^-$ by adding $Cl^-$ considerably can smooth the surface and can lead to the stabilization of the perovskite phase with compact, uniform and well-developed crystallites, which are important for the highly improved photoconductivity.

# References


[1] Lee M M, Teuscher J, Miyasaka T, Murakami T N and Snaith H J 2012 *Science* **338** 643
[2] Manser J S, Christians J A and Kamat P V 2016 *Chem. Rev.* **116** 12956
[3] Liu M, Johnston M B and Snaith H J 2013 *Nature* **501** 395
[4] Guo Z, Manser J S, Wan Y, Kamat P V and Huang L 2015 *Nat. Commun.* **6** 7471
[5] Xing G, Mathews N, Sun S, Lim S S, Lam Y M, Grätzel M, Mhaisalkar S and Sum T C 2013 *Science* **342** 344
[6] Etgar L, Gao P, Xue Z, Peng Q, Chandiran A K, Liu B, Nazeeruddin M K and Grätzel M 2012 *J. Am. Chem. Soc.* **134** 17396
[7] Saliba M, Matsui T, Seo J, Domanski K, Correa-Baena J P, Nazeeruddin M K, Zakeeruddin S M, Tress W, Abate A, Hagfeldt A, and Grätzel M 2016 *Energy Environ. Sci.* **9** 1989
[8] Jeon N J, Na H, Jung E H, Yang T Y, Lee Y G, Kim G, Shin H, Seok S, Lee J and Seo J 2018 *Nat. Energy* **3** 682
[9] Ren Y, Ding X, Wu Y, Ren Y K, Ding X H, Wu Y H, Zhu J, Hayat T, Alsaedi A, Xu Y, Li Z, Yang S and Dai S Y 2017 *J. Mater. Chem. A* **5** 20327
[10] Ren Y, Shi X, Ding X, Zhu J, Hayat T, Alsaedi A, Li Z, Xu X, Yang S and Dai S Y 2018 *Inorg. Chem. Front.* **5** 348
[11] Ren Y, Duan B, Xu Y, Huang Y, Li Z, Hu L, Hu L, Hayat T, Wang X, Zhu J and Dai S 2017 *Sci. Chin. Mater.* **60** 392
[12] Lin K, Xing J, Quan L, de Arquer F P G, Gong X, Lu J, Xie L, Zhao W, Zhang D, Yan C, Li W, Liu X, Lu Y, Kirman J, Sargent E H, Xiong Q and Wei Z 2018 *Nature* **562** 245
[13] Luo J, Wang X, Li S, Liu J, Guo Y, Niu G, Yao L, Fu Y, Gao L, Dong Q, Zhao C, Leng M, Ma F, Liang W, Wang L, Jin S, Han J, Zhang L, Etheridge J, Wang J, Yan Y, Sargent E H and Tang J 2018 *Nature* **563** 541
[14] Ivanovska T, Dionigi C, Mosconi E, De Angelis F, Liscio F, Morandi V and Ruani G 2017 *J. Phys. Chem. Lett.* **8** 3081
[15] Zhu X Y and Podzorov V 2015 *J. Phys. Chem. Lett.* **6** 4758
[16] Motta C and Sanvito S 2018 *J. Phys. Chem. C* **122** 1361
[17] McMeekin D P, Sadoughi G, Rehman W, Eperon G E, Saliba M, Hörantner M T, Haghighirad A, Sakai N, Korte L, Rech B, Johnston M B, Herz L M and Snaith H J 2016 *Science* **351** 151
[18] Jeon N J, Noh J H, Yang W S, Kim Y C, Ryu S, Seo J and Seok S I 2015 *Nature* **517** 476
[19] Mei A, Li X, Liu L, Ku Z, Liu T, Rong Y, Xu M, Hu M, Chen J, Yang Y, Grätzel M and Han H 2014 *Science* **345** 295
[20] Pei Y, Zou X, Guan Y and Teng G 2016 *Int. J. Photoenergy* **2016** 2953592
[21] Stranks S D, Eperon G E, Graneini G, Menelaou C, Alcocer M J P, Leijtens T, Herz L M, Petrozza A and Snaith H J 2013 *Science* **342** 341
[22] Karakus M, Jensen S A, D'Angelo F, Turchinovich D, Bonn M and Canovas E 2015 *J. Phys. Chem. Lett.* **6** 4991
[23] Ulbricht R, Hendry E, Shan J, Heinz T F and Bonn M 2011 *Rev. Mod. Phys.* **83** 543
[24] Noh J H, Im S H, Heo J H, Mandal T N and Seok S I 2013 *Nano Lett.* **13** 1764
[25] Papavassiliou G C, Pagona G, Karousis N, Mousdis G A, Koutselas I and Vassilakopoulou A 2012 *J. Mater. Chem.* **22** 8271
[26] Qiu J, Qiu Y, Yan K, Zhong M, Mu C, Yan H and Yang S 2013 *Nanoscale* **5** 3245
[27] Mosconi E, Amat A, Nazeeruddin M K, Grätzel M and De Angelis F 2013 *J. Phys. Chem. C* **117** 13902
[28] Guo X, McCleese C, Kolodziej C, Samia A C, Zhao Y and Burda C 2016 *Dalton Trans.* **45** 3806
[29] Schmuttenmaer C A 2004 *Chem. Rev.* **104** 1759
[30] Joyce H J, Bol, J L, Davies C L, Baig S A and Johnston M B 2016 *Semicond. Sci. Technol.* **31** 103003
[31] Ponseca Jr C S, Savenije T J, Abdellah M, Zheng K, Yartsev A, Pascher T, Harlang T, Chabera P, Pullerits T, Stepanov A, Wolf J and Sundstrom V 2014 *J. Am. Chem. Soc.* **136** 5189
[32] Marchioro A, Teuscher J, Friedrich D, Kunst M, Krol R, Moehl T, Grätzel M and Moser J 2014 *Nat. Photon.* **8** 250
[33] Yan H J, Ku Z L, Hu X F, Zhao W Y, Zhong M J, Zhu Q B, Lin X, Jin Z M and Ma G H 2018 *Chin. Phys. Lett.* **35** 028401
[34] Zhang Z, Lin T, Xing X, Lin X, Meng X, Cheng Z, Jin Z and Ma G 2017 *Appl. Phys. Lett.* **110** 111108
[35] Jensen S A, Mics Z, Ivanov I, Varol H S, Turchinovich D, Koppens. H L F, Bonn M and Tielrooij K J 2014 *Nano Lett.* **14** 5839
[36] Bretschneider S A, Ivanov I, Wang H I, Miyata K, Zhu X and Bonn M 2018 *Adv. Mater.* **30** 1707312
[37] Ponseca Jr C S, Tian Y, Sundström V and Scheblykin I G 2016 *Nanotechnology* **27** 082001
[38] Wehrenfennig C, Eperon G E, Johnston M B, Snaith H J and Herz L M 2014 *Adv. Mater.* **26** 1584
[39] Johnston M B and Herz L M 2016 *Acc. Chem. Res.* **49** 146
[40] Yan H, An B, Fan Z, Zhu X, Lin X, Jin Z and Ma G 2016 *Appl. Phys. A* **122** 414
[41] Yang Y, Yan Y, Yang M, Choi S, Zhu K, Luther J M and Beard M C 2015 *Nat. Commun.* **6** 7961
[42] Ghosh T, Aharon S, Etgar L and Ruhman S 2017 *J. Am. Chem. Soc.* **139** 18262
[43] Jha A, Duan H G, Tiwari V, Nayak P K, Snaith H J, Thorwart M and Miller R D 2018 *ACS Photon.* **5** 852
[44] Frost J M 2017 *Phys. Rev. B* **96** 195202
[45] Sendner M, Nayak P K, Egger D A, Beck S, Müller C, Epding B, Kowalsky W, Kronik L, Snaith H J, Pucci A and Lovrinčić R 2016 *Mater. Horizons* **3** 613
[46] Glover I I I R E and Tinkham M 1957 *Phys. Rev.* **108** 243
[47] Jin Z, Gehrig D, Dyer-Smith C, Heilweil E J, Laquai F, Bonn M and Turchinovich D 2014 *J. Phys. Chem. Lett.* **5** 3662

**Supplementary Material:**

# Ultrafast carrier dynamics and terahertz photoconductivity of mixed-cation and lead mixed-halide hybrid perovskites

Wan-Ying Zhao(赵婉莹)[1], Zhi-Liang Ku(库治良)[2], Li-Ping Lv(吕丽萍)[3], Xian Lin(林贤)[1], Yong Peng(彭勇)[2], Zuan-Ming Jin(金钻明)[1,4**], Guo-Hong Ma(马国宏)[1,4**], Jian-Quan Yao(姚建铨)[5]

[1] Department of Physics, Shanghai University, Shanghai 200444, China

[2] State key laboratory of advanced technology for materials synthesis and processing, Wuhan University of Technology, 122 Luoshi Road, Wuhan 430070, People's Republic of China

[3] Department of Chemical Engineering, School of Environmental and Chemical Engineering, Shanghai University, 99 Shangda Road, 200444 Shanghai, China.

[4] STU & SIOM Joint Laboratory for superintense lasers and the applications, Shanghai 201210, China

[5] College of Precision Instrument and Opto-electronics Engineering, Institute of Laser and Opto-electronics, Tianjin University, Tianjin 300072, People's Republic of China

**Correspondence author. Email: physics_jzm@shu.edu.cn; ghma@staff.shu.edu.cn

The samples were characterized by X-ray diffraction (XRD) spectra, as shown in Fig. S1. XRD revealed $14.1^{o}$ and $28.2^{o}$ peaks for (110) and (220) respectively, which is characteristic for the pristine perovskite with tetragonal crystal structure at room temperature[1,2].

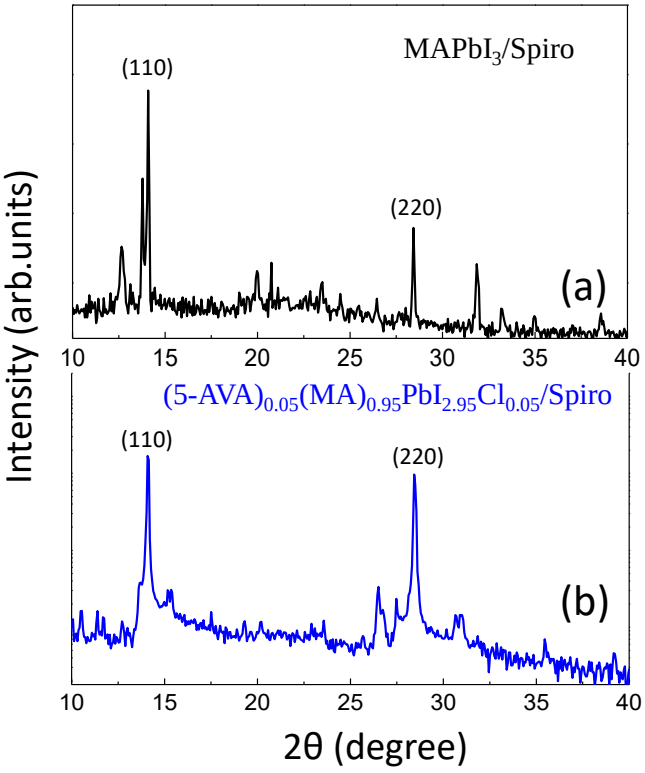


**Figure S1:** The characterization of the thin films of XRD spectra of MAPbI/s and (5-AVA)(MA)PbICl/s.

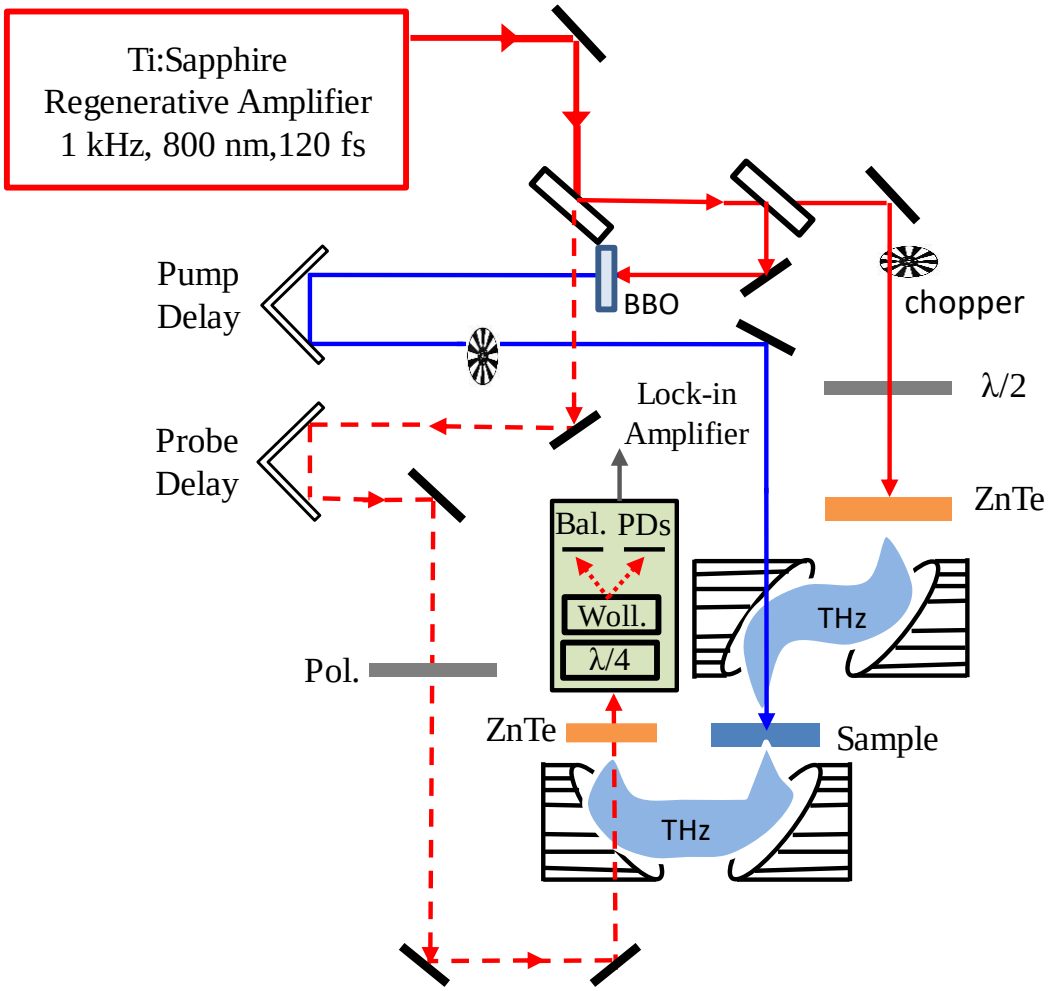


**Figure S2:** Experimental schemes of the Optical-pump THz-probe for the transmitted geometry. Pol: Polarizer, Bal. PDs: Balanced photo-detector, Woll.: Wollaston prism, λ/2: half-wave plate, λ/4: quarter-wave plate, BBO: β-$BaB_2O_4$ crystal.

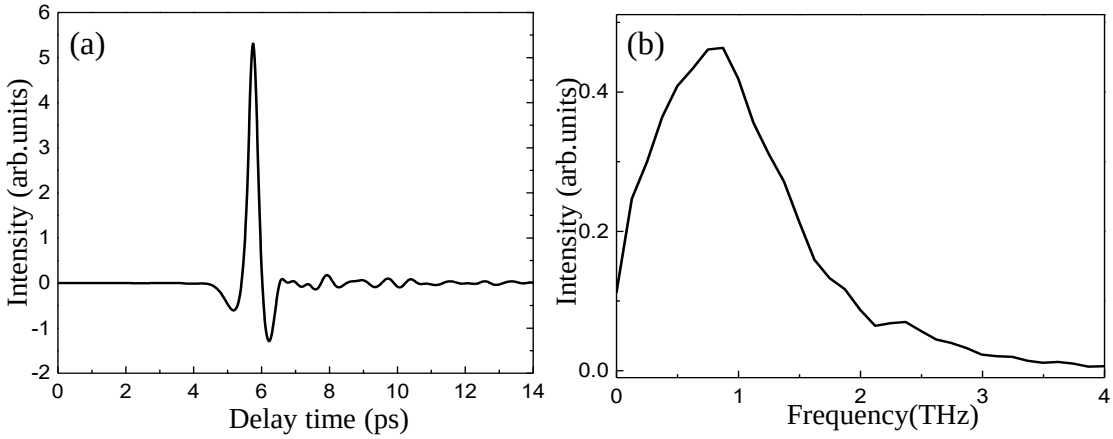


**Figure S3:** THz pulse generated from a 1-mm-thick (110)-orientated ZnTe crystals. (a) time-domain profile and (b) its frequency spectrum.

**References**

(1) Xin G, Christopher M, Charles K, Anna C S S, Yixin Z, Clemens B, 2016 *Dalton Trans.* **45** 3806

(2) Silvia C, Edoardo M, Paolo F, Andrea L, Francesco G, Fabio O, Patrizia F, Tullo B, Aurora R, Gianluca C, Giuseppe G, Filippo D A, Roberto M, 2013 *Chem. Mater.* **25** 4613